# Stochastic modulational instability in the nonlinear Schrödinger equation with colored random dispersion

Andrea Armaroli [1], Guillaume Dujardin [2], Alexandre Kudlinski,[1] Arnaud Mussot,[1] Stefano Trillo,[3] Stephan De Bièvre [4], and Matteo Conforti[1]

[1]*Univ. Lille, CNRS, UMR 8523-PhLAM-Physique des Lasers Atomes et Molécules, F-59000 Lille, France*
[2]*Univ. Lille, Inria, CNRS, UMR 8524 - Laboratoire Paul Painlevé, F-59000 Lille, France*
[3]*Department of Engineering, University of Ferrara, I-44122 Ferrara, Italy*
[4]*Univ. Lille, CNRS, Inria, UMR 8524 - Laboratoire Paul Painlevé, F-59000 Lille, France*

We study modulational instability (MI) in optical fibers with random group-velocity dispersion (GVD). We consider Gaussian and dichotomous *colored* stochastic processes. We resort to different analytical methods (namely, the cumulant expansion and the functional approach) and assess their reliability in estimating the MI gain of stochastic origin. If the power spectral density (PSD) of the GVD fluctuations is centered at null wave number, we obtain low-frequency MI sidelobes which converge to those given by a white-noise perturbation when the correlation length tends to 0. If instead the stochastic processes are modulated in space, one or more MI sidelobe pairs corresponding to the well-known parametric resonance (PR) condition can be found. A transition from small and broad sidelobes to peaks nearly indistinguishable from PR-MI is predicted, in the limit of large perturbation amplitudes and correlation lengths of the random process. We find that the cumulant expansion provides good analytical estimates for small PSD values and small correlation lengths, when the MI gain is very small. The functional approach is rigorous only for the dichotomous processes, but allows us to model a wider range of parameters and to predict the existence of MI sidelobes comparable to those observed in homogeneous fibers of anomalous GVD.

## I. INTRODUCTION

A physical system exhibiting an interplay of weak nonlinearity and group velocity dispersion (GVD) is subject to modulational instability (MI), i.e., the destabilization of a homogeneous state (plane or continuous waves), via the exponential growth of small harmonic perturbations on a uniform background [1]. After pioneering works on MI in electromagnetic waves [2], fluid mechanics [3,4], and plasmas [5], in the 1980s the phenomenon was observed in nonlinear fiber optics [6]. In uniform fibers, MI arises for anomalous (negative) GVD, but it may also appear for normal GVD if polarization [7], higher-order modes [8], or higher-order dispersion are considered [9]. A different kind of MI related to a parametric resonance (PR) mechanism emerges when the GVD or the nonlinearity of the fiber are periodically modulated [10–13].

The impact of a random variation of GVD on MI was also the subject of a considerable research effort. The particular case in which the GVD is perturbed by a Gaussian white noise, i.e., a process exhibiting a vanishing correlation length or equivalently a flat power spectral density (PSD), is exactly solvable [14–18]. When the unperturbed fiber has an anomalous GVD, the conventional MI gain profile is deformed due to the random perturbation. In addition, MI sidebands of stochastic origin appear in the case of normal GVD. A white noise, however, implies arbitrarily large variations of GVD on arbitrarily small scales: an idealization that does not always provide a relevant modeling of the randomness that may occur in physical fibers. A nonconclusive theoretical study of parametric amplification in the case of a GVD perturbed by a Gaussian process with a finite correlation length was proposed in [19], and a numerical study can be found in [20].

We aim at studying the MI problem in a class of random-GVD fibers that is both experimentally accessible and theoretically tractable. In [21], we studied the case of a GVD perturbed by randomly located sharp and large *kicks*. Two different families of random processes were chosen to generate their mutual spacing and amplitude. Different MI sidebands were predicted, including multibump ones around zero detuning and others localized around PR frequencies.

Here, we consider random fluctuations extended in space as in Ref. [14], but focus on *colored* processes exhibiting an exponentially decaying autocorrelation function. A low-pass (LP) and a band-pass (BP, modulated) case are considered. We resort to cumulant expansion [22–28], functional methods [29–31], and numerical simulations. The LP processes converge to the white-noise results for vanishing correlation lengths. The MI sidelobes are located in the same detuning range and have amplitudes of the same order of magnitude of those calculated from white noise. The BP processes yield PR-like MI sidebands that are also comparable (in their maximal values) to the white-noise MI gain. For this reason, the white noise turns out to be a reference for many crucial properties of the MI gain in a more generic setting, even though there is little hope of an experimental realization of it.

Since the values of frequency detuning span a large range, the validity of the different analytical methods has to be questioned, like in other physical settings and systems [32,33]. We thus have to rely on different approaches and comparatively assess their soundness in describing the different features of the MI sidelobes (position, height, width).

The rest of the paper is organized as follows. After presenting the model equations (Sec. II), we study in Sec. III the low-pass random fluctuation by means of the two different approaches mentioned above. We then analyze in Sec. IV band-pass random fluctuations, for which we find convenient to introduce an averaging approach to the stochastic equations. In each case we present a thorough comparison of analytical approaches to numerical results. To close the paper, we report our conclusions and perspectives.

## II. MODEL DESCRIPTION

The propagation of optical pulses in a nonlinear optical fiber can be modeled by the universal nonlinear Schrödinger equation (NLSE)

$$i\partial_z U - \frac{1}{2}\beta_2(z)\partial_{tt}U + \gamma|U|^2 U = 0. \quad (1)$$

Here $U(z, t)$ is the envelope of the optical pulse field in units of $\sqrt{W}$, function of the propagation distance $z$ and time $t$ in the frame of reference propagating at the group velocity of the mode propagating in the fiber, $\beta_2$ is the GVD, and $\gamma$ is the nonlinear coefficient [34]. They depend, respectively, on the dispersion relation and electromagnetic field profile of the fundamental mode propagating in the optical fiber. We suppose that $\beta_2$ fluctuates randomly in $z$, while $\gamma$ stays constant. This is reasonable if we consider an optical fiber operating near the zero-dispersion point, where the dispersion relation is very sensitive to geometry and refractive index contrast, but the confinement of light in the mode is not.

Let $\beta_2(z) = \beta_2^0 + \delta\beta(z)$, where $\beta_2^0 > 0$ (normal average GVD) and $\delta\beta(z)$ is a stochastic process of zero mean, that we specify below. We observe that, for $\delta\beta = 0$, Eq. (1) has a continuous wave ($t$-independent) solution $U_0(z) = \sqrt{P}\exp(i\gamma Pz)$.

In order to study the stability of this continuous-wave solution, we insert in Eq. (1) the perturbed solution $U(z, t) = [\sqrt{P} + \check{x}_1(z, t) + i\check{x}_2(z, t)]\exp(i\gamma Pz)$, linearize and Fourier transform the resulting equation with respect to $t$ ($\omega$ is used as the associated angular frequency detuning from the carrier $U_0$), to obtain

$$\frac{dx}{dz} = \begin{bmatrix} 0 & -g(z) \\ h(z) & 0 \end{bmatrix} x, \quad (2)$$

with $x \equiv (x_1, x_2)^{\mathrm{T}}$ (functions of $\omega$ and $z$), $g(z) = g_0 + \delta g(z)$, and $h(z) = h_0 + \delta g(z)$, with $g_0 \equiv \beta_2^0\frac{\omega^2}{2}$, $h_0 \equiv g_0 + 2\gamma P$, and $\delta g(z) \equiv \delta\beta(z)\frac{\omega^2}{2}$. Equation (2) is a system of stochastic differential equations (SDEs) for each value $\omega$. In the following sections we will discuss how to reduce it to a system of ordinary differential equations (ODEs) for the first and second moments of the probability density function of $x$ in order to estimate the MI gain.

We recall that we consider only normal average GVD, thus,

$$k^2 \equiv g_0 h_0 > 0 \quad (3)$$

and no conventional MI appears for $\delta\beta(z) = 0$. The MI sidebands we predict below are therefore completely ascribed to random fluctuations. The case of anomalous average GVD will be the subject of future work.

We focus here on two families of random processes, where the stochastic process $\delta\beta$ is characterized by two parameters $N_0 > 0$ and $B > 0$. The first family, for which we denote $\delta\beta \equiv \chi$, is characterized by an autocorrelation function of the form

$$R_\chi(\zeta \equiv z - z') \equiv \langle\chi(z)\chi(z')\rangle = \frac{N_0 B}{4}\exp(-B|\zeta|). \quad (4)$$

We recall that the variance of the process is $\sigma_\chi^2 = R_\chi(0) = \frac{N_0 B}{4}$. For $B \to \infty$, $R_\chi \to \frac{N_0}{2}\delta(\zeta)$, i.e., the white-noise autocorrelation function. Different stochastic processes exhibit this same autocorrelation function. Here, we consider the Gaussian (often denoted in the physics literature as Ornstein-Uhlenbeck [28]) and the dichotomous processes, which find important applications in physics and allow us to obtain workable approximations [33].

Both are stationary in $z$. By virtue of the Wiener-Khinchin theorem, the PSD of $\chi$ coincides with the Fourier transform of $R_\chi$:

$$S_\chi(\kappa) = \int_{-\infty}^{\infty}d\zeta\,R_\chi(\zeta)\exp(i\kappa\zeta) = \frac{N_0}{2}\frac{B^2}{B^2 + \kappa^2}. \quad (5)$$

The Gaussian process is numerically generated in the $\kappa$ domain by filtering an approximated white noise of PSD $N_0/2$ by means of a *low-pass* filter of transfer function

$$H_{\mathrm{LP}}(\kappa) = \frac{B}{B + i\kappa}. \quad (6)$$

The dichotomous process is more conveniently obtained directly in the $z$ domain by switching the amplitude of the fluctuation between $\pm\sigma_\chi$ with an exponentially distributed *waiting* (i.e., between switching points) length with mean $2/B$. Both are pertinent to fiber optics. Indeed, the Gaussian process corresponds to a continuous variation of GVD as can be obtained by varying the fiber radius during the drawing process. The dichotomous process corresponds to splicing together fibers with different GVD $\beta_2 = \beta_2^0(1 \pm \sigma_\chi)$ and random lengths. We refer to the processes belonging to this class, with autocorrelation function as in Eq. (4) and PSD as in Eq. (6) as LP processes.

The second family of stochastic processes, for which we denote $\delta\beta \equiv \xi$, is obtained as the modulated version of $\chi$ with central wave number $\kappa_0 = \frac{2\pi}{\Lambda_0} > 0$ ($\Lambda_0$ is the associated spatial period), that is written in phase-quadrature representation

$$\xi(z) = \psi_1(z)\cos\kappa_0 z + \psi_2(z)\sin\kappa_0 z. \quad (7)$$

Here, $\psi_{1,2}$ are two stationary (in $z$) and independent random processes with zero mean and autocorrelation functions

$$R_{\psi_i}(\zeta) = \frac{N_0 B}{2}\exp(-B|\zeta|), \quad (8)$$

for $i = 1, 2$; moreover, $\langle\psi_i\psi_j\rangle = \frac{N_0 B}{2}\delta_{ij}$. In analogy to $\chi$, we consider either two Gaussian or two dichotomous processes for $\psi_{1,2}$. They are generated according to their distribution as is done for $\chi$. The process $\xi$ thus exhibits an autocorrelation

function of the form

$$R_\xi(\zeta) = \frac{N_0 B}{2} \cos \kappa_0 \zeta \, \exp(-B|\zeta|). \tag{9}$$

The variance of the process is $\sigma_\xi^2 = \frac{N_0 B}{2}$, like for $\psi_{1,2}$.

The PSD of $\xi$ reads as

$$S_\xi(\kappa) = \frac{N_0}{2} \left[ \frac{B^2}{B^2 + (\kappa - \kappa_0)^2} + \frac{B^2}{B^2 + (\kappa + \kappa_0)^2} \right]. \tag{10}$$

We note that, for $B \ll \kappa_0$, $S_\xi$ is centered approximately around the wave number $\pm\kappa_0$, with $S_\xi(\pm\kappa_0) \approx \frac{N_0}{2} = S_\chi(0)$ and bandwidth $B$ (in wave number units). We refer to this family with autocorrelation function as in Eq. (9) and PSD as in Eq. (10) as BP processes.

For both LP and BP families, we employ the definition of correlation length [35] $\zeta^c \equiv \frac{1}{R(0)} \int_0^\infty d\zeta |R(\zeta)|$, which gives $\zeta_\chi^c = 1/B$ for $\chi$ and $\zeta_\xi^c \approx 2/(\pi B)$ for $\xi$, if $B \ll \kappa_0$.

In the next two sections we will study the effect $\chi$ and $\xi$, respectively, on the MI predicted by Eq. (2).

## III. LOW-PASS RANDOM DISPERSION

First we consider processes with the autocorrelation function given in Eq. (4). We will discuss both the first and the second moment equations associated to Eq. (2).

### A. Cumulant expansion (first moments)

The cumulant expansion yields a series development for the ODEs associated to a SDE [28]. It is similar to the Dyson series of scattering theory [36] and provides a solid base for

more *ad hoc* schemes [22]. See [26] for a systematic derivation of terms to arbitrary order.

Let us rewrite Eq. (2) in the standard form $\dot{x} = [A_1 + \alpha\eta(z)C_1]x$ with

$$A_1 = \begin{bmatrix} 0 & -g_0 \\ h_0 & 0 \end{bmatrix}, \quad C_1 = \begin{bmatrix} 0 & -1 \\ 1 & 0 \end{bmatrix},$$

$\alpha = \frac{\omega^2}{4}\sqrt{N_0 B}$ and $\eta = 2\chi/\sqrt{N_0 B}$ a random process with unit variance and zero mean. The expansion is performed in the formal parameter $\alpha$. To second order (the first-order term is obviously 0), we write the ODE for the first moment $\langle x \rangle = (\langle x_1 \rangle, \langle x_2 \rangle)^T$ as

$$\frac{d}{dz}\langle x \rangle = [A_1 + \alpha^2 K_2^1]\langle x \rangle, \tag{11}$$

with

$$K_2^1 = \int_0^\infty d\zeta \, C_1 e^{A_1 \zeta} C_1 e^{-A_1 \zeta} R_\eta(\zeta). \tag{12}$$

Other terms can be added in the expansion of Eq. (11): their contribution to the solution rapidly decreases if

$$\varepsilon \equiv \alpha\zeta^c \tag{13}$$

is small, i.e., $\frac{\omega^2}{4}\sqrt{\frac{N_0}{B}} \ll 1$. For large detuning or small filter bandwidth $B$, the approximation may be invalid. A fixed initial condition $x(0)$ can be considered and the solutions of Eq. (11) do not keep memory of it for $z \gg \zeta_c$. The long-term dynamics being our main focus, we set the limit of integration to infinity in Eq. (12) (see [25]).

By tedious but straightforward algebra, we obtain

$$\frac{d}{dz}\langle x \rangle = \begin{bmatrix} -\frac{\omega^4}{4}\frac{g_0}{2k^2}[(g_0 + h_0)c_1 - (h_0 - g_0)c_2] & -g_0 + \frac{\omega^4}{8k}(h_0 - g_0)c_3 \\ h_0 + \frac{\omega^4}{8k}(h_0 - g_0)c_3 & -\frac{\omega^4}{4}\frac{h_0}{2k^2}[(g_0 + h_0)c_1 + (h_0 - g_0)c_2] \end{bmatrix}\langle x \rangle, \tag{14}$$

with

$$c_1 \equiv \int_0^\infty d\zeta \, R_\chi(\zeta) = \frac{1}{2}S_\chi(0) = \frac{N_0}{4},$$

$$c_2 \equiv \int_0^\infty d\zeta \, R_\chi(\zeta)\cos 2k\zeta = \frac{1}{2}S_\chi(2k) = \frac{N_0 B^2}{4}\frac{1}{B^2 + 4k^2},$$

$$c_3 \equiv \int_0^\infty d\zeta \, R_\chi(\zeta)\sin(2k\zeta) = \frac{N_0 Bk}{2}\frac{1}{B^2 + 4k^2}. \tag{15}$$

Since $c_i > 0$, $i = 1, 2, 3$, for all $\omega$, and $c_1 > c_2$, it is easy to verify that the eigenvalues of the matrix in Eq. (14) have both a negative real part, so that the system (14) does not predict any MI gain. This finding is analogous to the conventional harmonic oscillator with random frequency [28,33], for which the first moment undergoes only damping. For this reason it is necessary to resort to the equations for the second moments.

We recall that, for white noise, the cumulant expansion at second order is exact and in that limit $B \to \infty$, $c_1 = c_2$ and $c_3 = 0$, so the eigenvalues of Eq. (14) reduce to Eq. (23) of Ref. [14].

### B. Cumulant expansion (second moments)

We now consider second moments. First we let $X_1 = x_1^2$, $X_2 = x_2^2$, and $X_3 = x_1 x_2$ and derive from Eq. (2) a system for their evolution, which reads as

$$\frac{d}{dz}X = \begin{bmatrix} 0 & 0 & -2g(z) \\ 0 & 0 & 2h(z) \\ h(z) & -g(z) & 0 \end{bmatrix}X. \tag{16}$$

In order to perform the cumulant expansion, we write Eq. (16) in standard form by letting

$$A_2 = \begin{bmatrix} 0 & 0 & -2g_0 \\ 0 & 0 & 2h_0 \\ h_0 & -g_0 & 0 \end{bmatrix}, \quad C_2 = \begin{bmatrix} 0 & 0 & -2 \\ 0 & 0 & 2 \\ 1 & -1 & 0 \end{bmatrix},$$

the other quantities $\alpha$ and $\eta$ being the same as in the previous subsection.

Up to second order, the cumulant expansion reads as

$$\frac{d}{dz}\langle X \rangle = [A_2 + \alpha^2 K_2^2]\langle X \rangle,$$

$$\text{with } K_2^2 = \int_0^\infty d\zeta \, C_2 e^{A_2 \zeta} C_2 e^{-A_2 \zeta} R_\eta(\zeta), \tag{17}$$

which gives

$$
\frac{d}{dz}\langle X\rangle = \begin{bmatrix} -\frac{\omega^4}{4g_0}[(g_0+h_0)c_1 + (g_0-h_0)c_2] & \frac{\omega^4}{4h_0}[(g_0+h_0)c_1 - (g_0-h_0)c_2] & -2g_0 \\ \frac{\omega^4}{4g_0}[(g_0+h_0)c_1 + (g_0-h_0)c_2] & -\frac{\omega^4}{4h_0}[(g_0+h_0)c_1 - (g_0-h_0)c_2] & 2h_0 \\ h_0 + \frac{\omega^4}{4k}(h_0-g_0)c_3 & -g_0 + \frac{\omega^4}{4k}(h_0-g_0)c_3 & -\frac{\omega^4}{4k^2}[(g_0+h_0)^2c_1 - (g_0-h_0)^2c_2] \end{bmatrix}\langle X\rangle,
$$

(18)

with the $c_i$'s defined as above. The validity condition of the expansion is the same as in the previous subsection.

As in Ref. [21], the MI of stochastic origin is related to the growth rate of the second moment. The eigenvalues of the matrix in Eq. (18) can be written analytically. Their form is rather complicated: in general we have two complex-conjugate eigenvalues ($\lambda_\pm$) with negative real part and one positive real eigenvalue $\lambda_0$. The MI gain is thus defined as $G_2(\omega) \equiv \frac{\lambda_0}{2}$. Since $G_2(\omega)$ is small for small $N_0$, we proceed like in Ref. [14] to derive the following approximation:

$$
G_2(\omega) \approx \frac{4(\gamma P)^2 k\omega^4\{8c_2 k^3 + c_3\omega^4[c_1 j_0^2 - 4c_2(\gamma P)^2]\}}{64k^6 - 32c_3(\gamma P)^2 k^3\omega^4 - \omega^8[c_1 j_0^2 - 4c_2(\gamma P)^2]^2},
$$

(19)

with $j_0 \equiv g_0 + h_0$. Nevertheless, this expression is still very cumbersome and, below, we rely only on the numerically computed eigenvalue $\lambda_0$.

We note that the cumulant expansion could be extended to fourth order (the process being Gaussian, the third-order terms vanish), but the resulting terms are very involved and do not clarify the behavior of gain at large $\omega$, where the method breaks down (see below).

### C. Functional approach

An alternative approach follows [33,37] and generalizes the use of Furustu-Novikov-Shapiro-Loginov formulas, on which the treatment of white noise in Ref. [14] is based.

Let us consider one of the second moments $X_i$, $i = 1, 2, 3$. They are functionals of $\delta g$. Since $\delta g \propto \chi$, its autocorrelation function has the form of Eq. (4). According to Ref. [31], we have

$$
\left\langle \delta g \frac{dX_i}{dz} \right\rangle = \left( \frac{d}{dz} + B \right)\langle \delta g X_i\rangle.
$$

(20)

Two steps are needed to write an averaged system: (i) average directly Eq. (16); (ii) multiply each row by $\delta g$ and average. We introduce three new variables, $X_{3+i} \equiv \delta g X_i$ and, in order to truncate the system, we assume $\langle \delta g^2 X_i\rangle = \sigma_{\delta g}^2\langle X_i\rangle$, where $\sigma_{\delta g}^2 \equiv N_0 B \frac{\omega^4}{16}$ is the variance of the process. This last assumption is rigorously valid only for a dichotomous process [33] and in general an infinite hierarchy of equations is obtained for a Gaussian one (see [31]).

We obtain a sixth-order system of ODEs

$$
\frac{d}{dz}\langle X\rangle = \begin{bmatrix} 0 & 0 & -2g_0 & 0 & 0 & -2 \\ 0 & 0 & 2h_0 & 0 & 0 & 2 \\ h_0 & -g_0 & 0 & 1 & -1 & 0 \\ 0 & 0 & -2\sigma_{\delta g}^2 & -B & 0 & -2g_0 \\ 0 & 0 & 2\sigma_{\delta g}^2 & 0 & -B & 2h_0 \\ \sigma_{\delta g}^2 & -\sigma_{\delta g}^2 & 0 & h_0 & -g_0 & -B \end{bmatrix}\langle X\rangle.
$$

(21)

The matrix in Eq. (21) has six eigenvalues. We observe numerically that one is real and negative, one ($\lambda_0$) is real and positive, the last four are two pairs of complex-conjugate values with negative real part. The MI gain is defined as above, $G_2(\omega) \equiv \frac{\lambda_0}{2}$. By numerical inspection, we notice that the system in Eq. (21) generally gives different eigenvalues with respect to Eq. (18). We stress that, in contrast to Sec. III B, the accuracy of the functional approach does not require any condition on $\varepsilon$. However, in the white-noise limit of $B \to \infty$, the system reduces to three independent variables [33] and we obtain the Eqs. (26)–(30) of [14], which as expected coincide with the cumulant expansion results.

In the next subsection, we will show what are the limits of validity of the two approximations and which fits better to numerical results.

### D. Results

In order to validate our theoretical analysis, we resort to solving Eq. (2) by generating a large number $N$ of realizations of $\chi$ and studying the moments of the resulting sample of solutions. The solution of Eq. (2) is known exactly for piecewise constant $\beta_2(z)$ in terms of transfer matrices [34]. For the Gaussian process, we choose the length $L$ of the domain sufficiently large to ensure that the sampling rate in the spatial frequency, i.e., $\Delta\kappa = \frac{2\pi}{L}$, fairly represents the PSD of the process, namely, $B/\Delta\kappa \ll 1$. An array of identically distributed Gaussian random variables of zero mean and variance $\sigma^2 = \frac{N_0}{2\Delta z}$, with $\Delta z$ the sampling distance in $z$ (over which the dispersion is assumed constant), is generated numerically. This array is transformed to the $\kappa$ domain by means of FFT, then multiplied by the Lorentzian filter of Eq. (6) and transformed back to space domain. A realization of the dichotomous process is instead obtained in the $z$ domain, by randomly generating the switching distances (where $\chi$ changes sign) from a randomly generated exponential distribution of mean $2/B$. Between two switching points, the GVD is assumed constant.

We solve Eq. (2) for a given initial condition $(x_1(0), x_2(0))^{\mathrm{T}} = (1, 0)$, corresponding to balanced sidebands, over each random sequence of constant dispersion segments, to obtain a set of output vectors $(x_1(L), x_2(L))^{\mathrm{T}}$ from which we estimate the MI gain. Let $P_{\mathrm{out}} \equiv x_1^2(L) + x_2^2(L)$. We then compute the mean gain, defined as [20,21]

$$
G \equiv \frac{1}{2L} \ln\left\langle \frac{P_{\mathrm{out}}}{P_{\mathrm{in}}} \right\rangle.
$$

(22)

In all our results we take $\gamma P = \beta_2^0 = 1$. This is equivalent to putting Eq. (1) in the standard adimensional form.
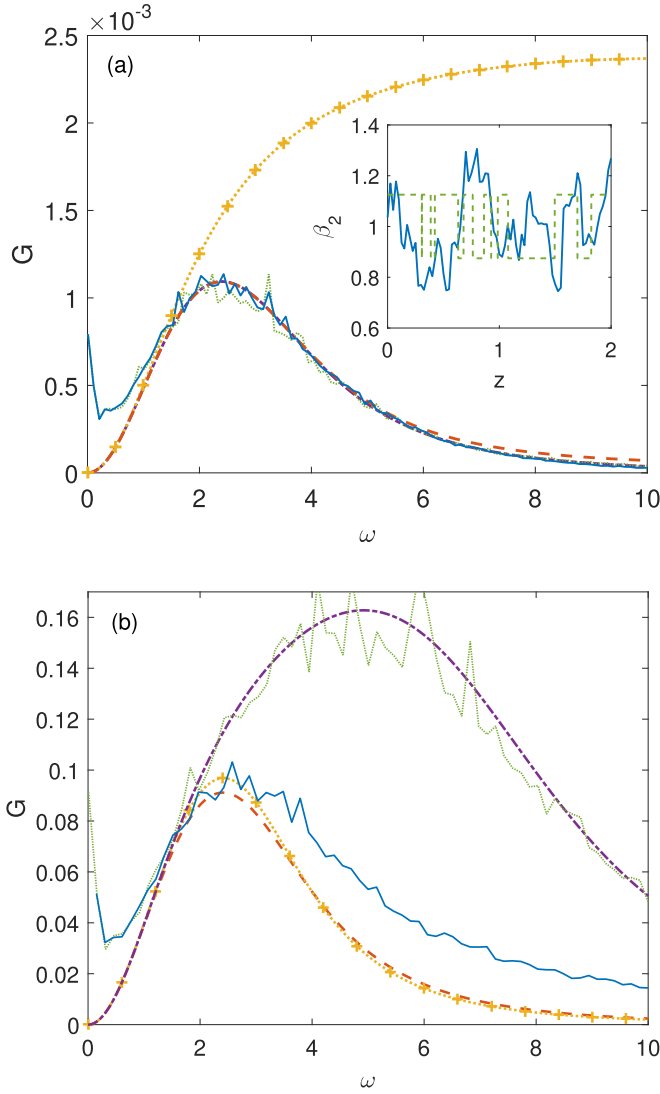
FIG. 1. MI gain as a function of detuning $\omega$ for a LP random dispersion. Comparison of numerical values for a Gaussian (blue solid lines) and dichotomous process (green dotted lines) obtained from Eq. (2) with the estimates provided by Eq. (18) (red dashed lines) and by Eq. (21) (dashed-dotted purple lines). We include also the gain corresponding to the white process (yellow dotted line with pluses). In (a) $N_0 = 0.005$ and $B = 4\pi$, so that $\varepsilon < 0.5$ over the considered $\omega$ range, (b) $N_0 = 0.4$ and $B = 4\pi$, so that $\varepsilon \approx 1$ around the maximum gain. The inset in (a) shows a single realization of the two processes.

In Fig. 1 we consider two examples of MI gain curves. We notice that the sidelobes exhibit a single maximum $G_{max}$ at detuning $\omega_{max}$.

We consider two different values of $N_0$. For small values, the gain is generally small [see Fig. 1(a)], where $N_0 = 0.005$. We choose a long domain $L = 5000$ to prevent finite-size effects that may appear at small $\omega$, where the transmission $P_{out}/P_{in}$ grows as a power law [38], and $\Delta z = 0.01$ for the Gaussian case. Satisfactory statistics are obtained for $N = 2000$.

In this case $\varepsilon \approx 0.5$ at $\omega = 10$ [see the definition of $\varepsilon$ in (13)], the cumulant expansion is thus expected to be valid. The functional approach gives very similar results, apart from some deviations in the large-$\omega$ tails. The numerical data show that the two processes provide the same trend, that matches almost perfectly with the analytical estimates (the functional approach proves more accurate in the tails, as expected). The behavior near $\omega = 0$ is due to the above-mentioned finite-size effects. We notice that the LP process provides a much narrower and smaller gain than the white noise (dotted yellow line with pluses). In this regime, the correlations of the stochastic process suppress the MI gain.

Then we study the case of an intermediate value $N_0 = 0.4$, where $\varepsilon > 1$. We choose $L = 50$, $\Delta z = 0.01$, and $N = 1000$. We show in Fig. 1(b) how the numerical results compare to the analytical estimates. The functional approach proves very accurate for the dichotomous process over the full range of $\omega$. The cumulant expansion models the numerical data quite well, except in the large-$\omega$ tails. We notice that the white-noise gain is smaller than the LP gain lobes, particularly for the dichotomous case. Thus, for large $N_0$, correlations can improve the MI gain.

In Figs. 2 and 3 we show the effect of variations of $B$ on $\omega_{max}$ and $G_{max}$, respectively; $L$, $\Delta z$, and $N$ are chosen to guarantee a satisfactory statistical sample for each point.

For $N_0 = 0.005$ [Figs. 2(a) and 3(a)] the position as well as the value of the maximum gain are, for both stochastic processes, in the same range of values and are, within the residual oscillation margins, well approximated by both methods. Both $\omega_{max}$ and $G_{max}$ are monotone increasing functions of $B$. As $B \to +\infty$, they converge from below to the corresponding values for a white-noise process. The limiting values are not shown because they are well beyond the axis scales.

The behavior for $N_0 = 0.4$ is very different [Figs. 2(b) and 3(b)]. First, for the dichotomous case, the numerical points are well approximated by the eigenvalues of Eq. (21). The maximum MI gain exhibits a sharp peak [see Fig. 3(b)]. We notice in Fig. 2(b) that $\omega_{max}$ diverges for this value of $B$: this means that the gain lobe never decays.

To understand this phenomenon, we study the eigenvalues of Eq. (21) at $\omega \to \infty$ and we notice that, for $\sigma_{\delta g} = g_0$, i.e., $B = 4(\beta_2^0)^2/N_0$, $G_2(\omega)$ converges, for small $N_0$, to $G_{max} \approx \frac{1}{4}[-B + \sqrt{\frac{B^2 + B\sqrt{B^2 + 64(\gamma P)^2}}{2}}]$. Notice also that for this value $\sigma_\chi^2 = 1$, i.e., in dimensional units the GVD switches from 0 to $2\beta_2^0$. In the present case, $B = 10$ and $G_{max} \approx 0.17$, as observed in Fig. 3(b). For $N_0 > 1$, the reasoning is still valid: the value of $B$ for which $G_2(\omega)$ does not decay at $\omega \to \infty$ is well predicted, while its value is generally larger than the approximated $G_{max}$ above. From a physical point of view, this case is very pathological because higher-order dispersion effects should be included in Eq. (1).

For the Gaussian process, $\omega_{max}$ and $G_{max}$ stay close to the white-noise limit (yellow dotted line) even for small $B$ and are satisfactorily described by the cumulant expansion for large $B$. As expected, the cumulant expansion is not accurate for small $B$ and is very different from the estimate of the functional approach.
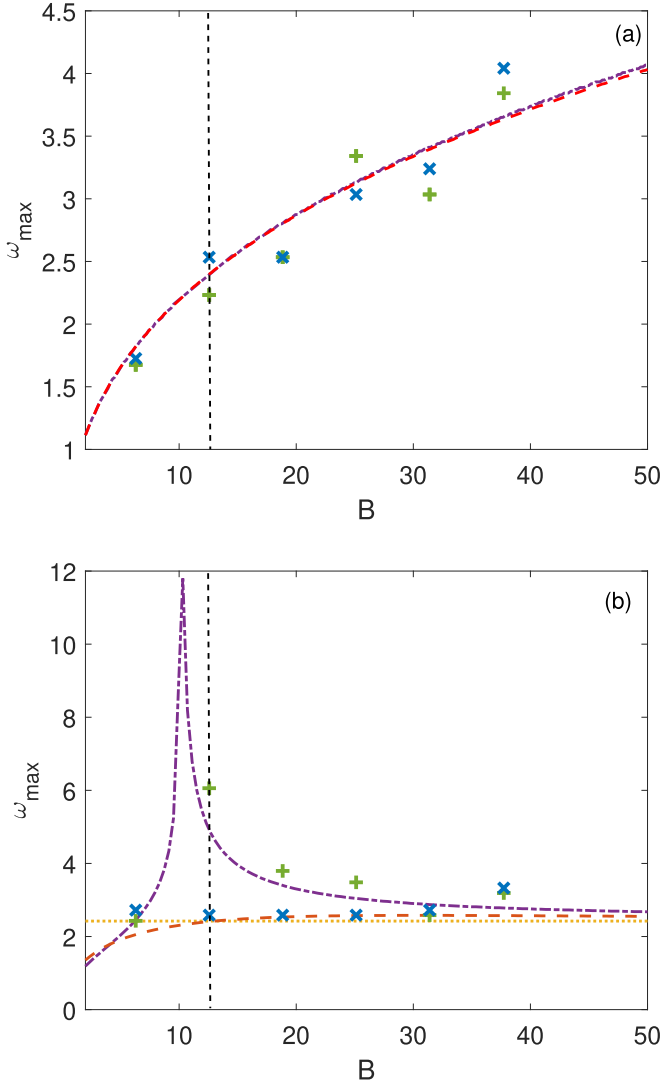
FIG. 2. Detuning at the gain maximum as a function of *B*. Numerical results of Gaussian (blue crosses) and dichotomous (green pluses) process are compared to Eq. (18) (red dashed line) and Eq. (21) (purple dashed-dotted line). We include $\omega_{\max}$ for the white noise, too, as reference (yellow dotted line). The dashed vertical lines highlight the value of *B* used in Fig. 1. (a) $N_0 = 0.005$, (b) $N_0 = 0.4$.

We conclude that the cumulant expansion provides an accurate approximation for $G_{\max}$ and $\omega_{\max}$ for the Gaussian process. We recall that, on the contrary, this is not the case for the behavior of the MI gain at large $\omega$ [see Fig. 1(b)].

In conclusion, the LP processes yield a very small gain for $\varepsilon \ll 1$, always less than white-noise limit. For $\varepsilon \sim 1$, $G_{\max}$ can yield an MI gain larger than the white-noise gain, but is about one order of magnitude smaller than the conventional MI gain in homogeneous fibers with anomalous GVD.

## IV. NARROW-BAND RANDOM DISPERSION

Here we consider the modulated process $\xi$ with the autocorrelation function in Eq. (9), for which a new degree of freedom $\kappa_0$ is included. We start directly from Eq. (16).
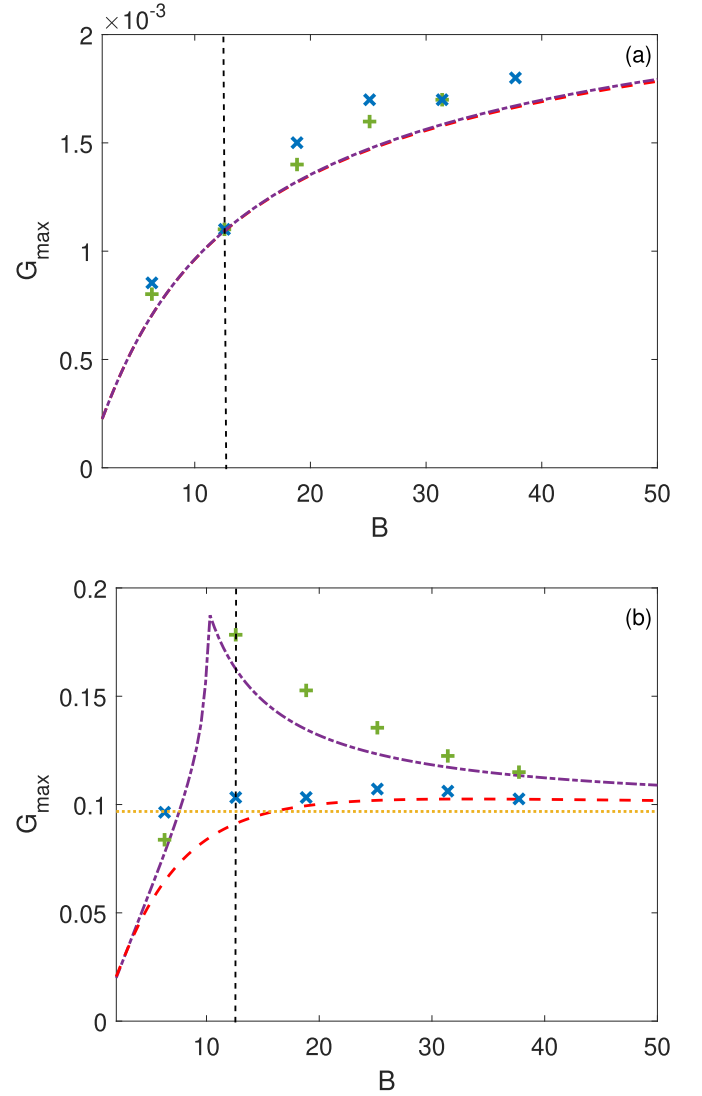


FIG. 3. Maximum gain as a function of *B*. Same convention as in Fig. 2.

## A. Direct cumulant expansion

The cumulant expansion gives the same result as Eq. (18) with

$$c_1 = \frac{N_0}{2} \frac{B^2}{B^2 + \kappa_0^2},$$

$$c_2 = \frac{N_0 B^2}{4} \left[ \frac{1}{B^2 + (2k - \kappa_0)^2} + \frac{1}{B^2 + (2k + \kappa_0)^2} \right],$$

$$c_3 = N_0 B \kappa \frac{B^2 - \kappa_0^2 + 4k^2}{[B^2 + (2k - \kappa_0)^2][B^2 + (2k + \kappa_0)^2]}. \quad (23)$$

We observe that, while $c_1$ is constant, $c_2$ and $c_3$ exhibit a resonant line-shape behavior close to $2k = \kappa_0$, i.e., the first PR condition: the former exhibits a maximum at $4k^2 \approx \kappa_0^2 - \frac{B^4}{4\kappa_0^2}$, while the latter crosses zero at $4k^2 = \kappa_0^2 - B^2$. We recall that the $m$th-order PR condition is in general $2k = m\kappa_0$, which

gives

$$\omega_{\mathrm{PR},m}^2 = \sqrt{4\left(\frac{\gamma P}{\beta_2^0}\right)^2 + \left(\frac{m\kappa_0}{\beta_2^0}\right)^2} - \frac{2\gamma P}{\beta_2^0}. \tag{24}$$

For $B \ll \kappa_0$, we can set $c_1 \approx 0$. Then, around the first parametric resonance detuning, tedious but straightforward calculations show that the instability gain is approximated by

$$G_2(\omega) \approx \frac{1}{2}\frac{(2\gamma P)^2\omega^4}{\kappa_0^2}c_2, \tag{25}$$

that attains its maximum approximately at $\omega_{\mathrm{PR},1}$,

$$\begin{aligned}
G_2^{\max} \approx G_2(\omega_{\mathrm{PR},1}) &\approx \frac{N_0(\gamma P)^2}{2}\frac{\omega_{\mathrm{PR},1}^4}{\kappa_0^2} \\
&= \frac{N_0(\gamma P)^2}{(2\beta_2^0)^2}\frac{\omega_{\mathrm{PR},1}^2}{\omega_{\mathrm{PR},1}^2 + \frac{4\gamma P}{\beta_2^0}}.
\end{aligned} \tag{26}$$

We remark also that Eq. (25) is composed of a Lorentzian factor depending on the process PSD ($c_2$) and a factor independent of the process. Moreover, it turns out that the maximum MI gain, Eq. (26), coincides, for small $\omega$ and a given $N_0$ with the white-noise MI gain evaluated at $\omega = \omega_{\mathrm{PR},1}$, as hinted at in Ref. [32].

Notice that in Eq. (26), the MI gain is proportional to $\frac{N_0\omega_{\mathrm{PR},1}^4}{\kappa_0^2}$, while the PR-MI scales like $\theta\frac{\omega_{\mathrm{PR},1}^2}{\kappa_0}$ [12], with $\theta$ the (constant) amplitude of the periodic variation. As in the low-pass case, according to Eq. (26) the maximal MI gain depends mainly on $N_0$. For $B \to 0$, the analogy to PR would suggest, instead, a dependence on the amplitude of the fluctuations in real space, i.e., $N_0B$, as discussed also in Ref. [32]. Below, we clarify this ostensible inconsistency.

## B. Near-resonance reduction

In analogy to Ref. [32], a significant simplification of Eq. (2) can be obtained by the conventional averaging method used for PR [39].

In order to average Eq. (2), we let

$$\begin{aligned}
x_1(z) &= y_1(z)\cos\left(\frac{\kappa_0}{2}z\right) + y_2(z)\sin\left(\frac{\kappa_0}{2}z\right), \\
x_2(z) &= \frac{\kappa_0}{2g_0}\left[y_1(z)\sin\left(\frac{\kappa_0}{2}z\right) - y_2(z)\cos\left(\frac{\kappa_0}{2}z\right)\right],
\end{aligned} \tag{27}$$

where $x_2$ is written assuming $g = g_0$ constant, in the spirit of the variation of constants.

By averaging out oscillating terms, noticing that $\frac{\delta g}{g_0} = \xi$, and employing the phase-quadrature representation of $\xi$ [see Eq. (7)], we obtain

$$\begin{aligned}
\kappa_0\dot{y}_1 &= \Delta^2 y_2 + \Gamma\psi_1 y_2 - \Gamma\psi_2 y_1, \\
\kappa_0\dot{y}_2 &= -\Delta^2 y_1 + \Gamma\psi_1 y_1 + \Gamma\psi_2 y_2,
\end{aligned} \tag{28}$$

with $\Gamma \equiv \frac{1}{2}(\frac{\kappa_0^2}{4} - g_0^2)$ and $\Delta^2 \equiv k^2 - \frac{\kappa_0^2}{4}$ quantifies the detuning from the PR condition; close to resonance, $\Delta^2 = (k + \kappa_0/2)(k - \kappa_0/2) \approx \kappa_0(k - \kappa_0/2)$.

Notice that the PR-MI gain of the first PR tongue is obtained from Eq. (28) by putting $\psi_1 = \psi_2 = \theta$. It reads as

$$G_{\mathrm{PR},1} = \frac{\sqrt{2(\Gamma\theta)^2 - \Delta^2}}{\kappa_0}. \tag{29}$$

Starting from Eq. (28), in this section we only study the evolution of second moments. We introduce $Y_1 \equiv y_1^2$, $Y_2 \equiv y_2^2$, and $Y_3 \equiv y_1 y_2$. It is easy to verify that $Y \equiv (Y_1, Y_2, Y_3)^{\mathrm{T}}$ obeys

$$\kappa_0\frac{d}{dz}Y = \begin{bmatrix} -2\Gamma\psi_2 & 0 & 2\Delta^2 + 2\Gamma\psi_1 \\ 0 & 2\Gamma\psi_2 & -2\Delta^2 + 2\Gamma\psi_1 \\ -\Delta^2 + \Gamma\psi_1 & \Delta^2 + \Gamma\psi_1 & 0 \end{bmatrix}Y, \tag{30}$$

where the parameters are the same as those used throughout this section.

Two random processes appear in Eq. (30) and both the cumulant expansion and functional approach need generalizing accordingly. While we present the former in Appendix, because it provides very similar results to the direct cumulant expansion of the previous subsection, the latter is reported below.

## C. Functional approach near resonance

Following [40], we generalize the functional approach. We define $Y_{3+i} \equiv \psi_1 Y_i$, $Y_{6+i} \equiv \psi_2 Y_i$, and $Y_{9+i} \equiv \psi_1\psi_2 Y_i$, $i = 1, 2, 3$. We perform four different averaging steps: (i) average directly Eq. (30), (ii) multiply each row of Eq. (30) by $\psi_1$ and average, (iii) multiply by $\psi_2$ and average; (iv) multiply by $\psi_1\psi_2$ and average. We employ the formula of differentiation in Eq. (20) and its generalization

$$\left\langle\psi_1\psi_2\frac{dY_i}{dt}\right\rangle = \left(\frac{d}{dt} + 2B\right)\langle\psi_1\psi_2 Y_i\rangle. \tag{31}$$

If we assume as above that we can factor the variance out if the same process occurs twice in an average, we obtain

$$\kappa_0\frac{d\langle Y\rangle}{dz} = \begin{bmatrix} A_2 & \Gamma C_2' & \Gamma C_2'' & \mathbf{0} \\ \sigma_\xi^2\Gamma C_2' & A_2 - B\mathbf{I} & \mathbf{0} & \Gamma C_2'' \\ \sigma_\xi^2\Gamma C_2'' & \mathbf{0} & A_2 - B\mathbf{I} & \Gamma C_2' \\ \mathbf{0} & \sigma_\xi^2\Gamma C_2'' & \sigma_\xi^2\Gamma C_2' & A_2 - 2B\mathbf{I} \end{bmatrix}$$
$$\times\langle Y\rangle, \tag{32}$$

with

$$A_2 = \begin{bmatrix} 0 & 0 & 2\Delta^2 \\ 0 & 0 & -2\Delta^2 \\ -\Delta^2 & \Delta^2 & 0 \end{bmatrix}, \quad C_2' = \begin{bmatrix} 0 & 0 & 2 \\ 0 & 0 & 2 \\ 1 & 1 & 0 \end{bmatrix},$$
$$C_2'' = \begin{bmatrix} -2 & 0 & 0 \\ 0 & 2 & 0 \\ 0 & 0 & 0 \end{bmatrix}, \tag{33}$$

and denoting $\mathbf{0}$ and $\mathbf{I}$ the null and identity matrix, respectively.

We compute numerically the eigenvalues of the matrix in Eq. (32) and look for the dominant one $\lambda^*$. The maximum MI gain, for $\Delta^2 = 0$, is found analytically as

$$\left(G_2^{\mathrm{PR}}\right)^{\max} = \frac{1}{4\kappa_0}\left[\sqrt{B^2 + 4N_0 B\omega_{\mathrm{PR},1}^4} - B\right]. \tag{34}$$

We remark that the dependence on $\sigma_\xi$ is different from Eq. (26). For small $B$, the gain is no longer proportional to

$\frac{\omega_{\mathrm{PR},1}^4 N_0}{\kappa_0^2}$, but to $\frac{\omega_{\mathrm{PR},1}^2 \sqrt{N_0 B}}{\kappa_0}$, as we would formally obtain in the conventional periodic dispersion case, once we replace the amplitude of parametric oscillation $\theta$ with $\sqrt{2}\sigma_\xi$.

Thus, a very different result is found when compared to the cumulant expansions above. We now assess which approximation works better by comparing them to numerical solutions of Eq. (2).

### D. Results

In order to generate a realization of the process $\xi$ with Gaussian distribution (respectively dichotomous), we employ the same approach in the spectral (respectively spatial) domain as above, generate two independent LP processes, and modulate them according to Eq. (7). The numerical domain is obviously discretized in both cases: for the Gaussian process a lower limit on $L$ is required as in Sec. III D, the dichotomous process requires a short $\Delta z$ to avoid spurious correlations. We do not forget to correctly sample the period $\Lambda_0$ of the process spatial oscillations.

While in the previous section we were interested in the limit $B \to \infty$ to contrast the LP processes to white noise, here we aim at understanding the opposite limit $B \to 0$, with fixed and finite $N_0 B$. We expect that the gain associated to the stochastic fluctuations converges to the one of the periodically modulated fiber in this limit.

First, we consider a small perturbation $N_0 = 0.005$, with an intermediate bandwidth $B = \pi/4$ around $\kappa_0 = 2\pi$. We take $L = 500$, $\Delta z = 0.01$; a consistent statistical sample is collected for $N = 2000$. In Fig. 4(a) we compare the numerical mean gain $G(\omega)$ with the analytical estimates obtained above. For such a small perturbation, only a single MI peak can be observed (see the inset for a larger detuning range). We notice that the MI gain is centered about $\omega_{\mathrm{PR},1}$ with gain $G_{\max}$ and width $\Delta\omega$. The Gausssian and dichotomous processes give two almost identical results. The cumulant expansion provides a very good approximation because $\varepsilon \approx 0.1$. The near-resonance functional approach proves instead very imprecise, as far as both $G_{\max}$ and $\Delta\omega$ are concerned. We explain this as follows: It is easy to verify that the period of the modulation is comparable to correlation length $\Lambda_0 \approx \zeta_c$. Thus, we apply successively two distinct averaging procedures (near-resonant expansion and functional approach) upon two perturbations occurring at the same scale as if they were independent. This is a sure recipe for failure.

Moreover, we are not showing here the result of Eq. (A3) that coincides with the direct cumulant expansion around $\omega_{\mathrm{PR},1}$, but is skewed towards $\omega \to 0$, contrary to the numerical results.

As a second case, we consider a large $N_0 = 3.2$ and a small bandwidth $B = \pi/32$. All the other parameters are the same as the previous. In Fig. 4(b) we observe, as above, that the MI lobe occurs around $\omega_{\mathrm{PR},1}$ and the Gaussian and dichotomous processes provide two very close results. For such a large perturbation, several MI sidelobes can be observed, in analogy to PR-MI [see the inset of Fig. 4(b)]. Now $\varepsilon \approx 6.3 \gg 1$; we thus expect that the cumulant expansion fails to correctly describe the numerical results: indeed, it overestimates the peak MI while it underestimates its width (red dashed line). It captures
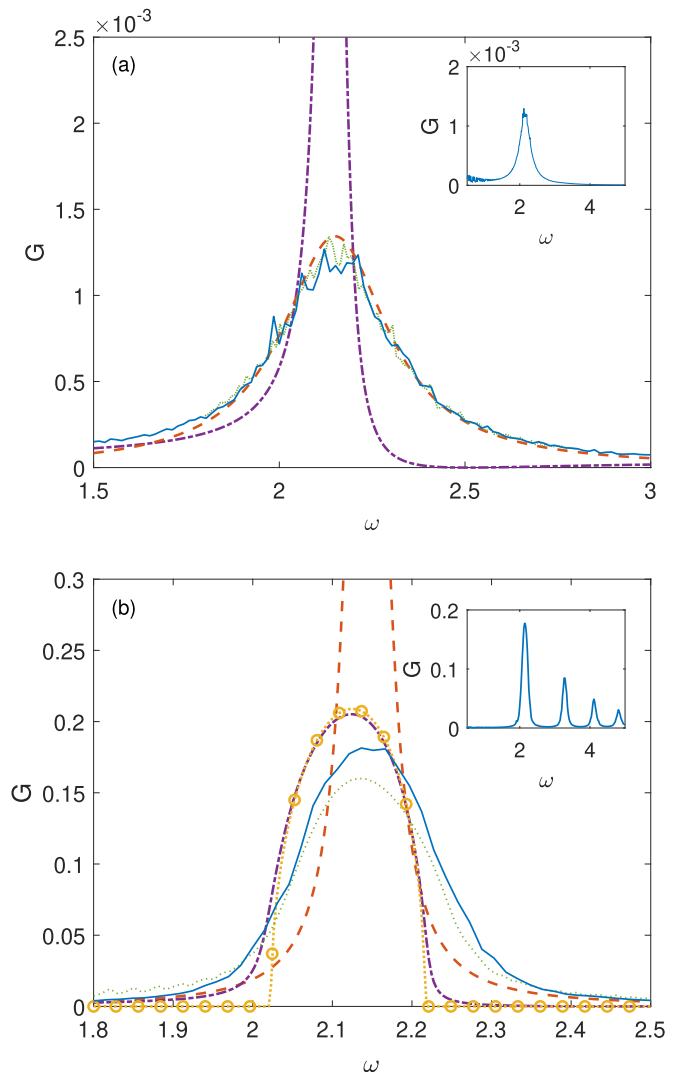


FIG. 4. MI gain as a function of detuning $\omega$ for a BP random dispersion $\kappa_0 = 2\pi$. Comparison of numerical values for a Gaussian (blue solid lines) and dichotomous process (green dotted lines) obtained from Eq. (2) with the estimates provided by Eqs. (18) and (23) (red dashed lines), and by Eq. (32) (dashed-dotted purple lines). In (a) $N_0 = 0.005$ and $B = \pi/4$, so that $\varepsilon < 0.1$ around the PR resonance, (b) $N_0 = 3.2$ and $B = \pi/32$, so that $\varepsilon \gg 1$ around the $\omega_{\max}$. In (b), we include the PR-MI gain of Eq. (29) with $\theta = \sqrt{2}\sigma_\xi = \sqrt{\pi/5}$ (yellow dotted line with circles). The insets show the numerical results for a Gaussian process on a larger $\omega$ range.

approximately the behavior of the MI gain in the tails (both left- and right-hand sides). The functional method provides instead a good approximation (purple dashed-dotted line). For these parameters, Eq. (32) provides a result very close to the conventional PR gain (yellow dotted line with circles) apart from the tails. We can thus state that for $\zeta_c \gg \Lambda_0$, the proposed functional approach gives a good estimate of the numerically estimated mean gain because the two independent approximations are performed in the correct order on the two different scales, i.e., for $B \ll \kappa_0$, the BP process can be considered a small perturbation to the PR-MI effect. We show in Fig. 5 the effect of variations of $B$ on $G_{\max}$. We keep $\kappa_0$ and $N_0 B$ constant; $L$, $\Delta z$, and $N$ are chosen to guarantee a
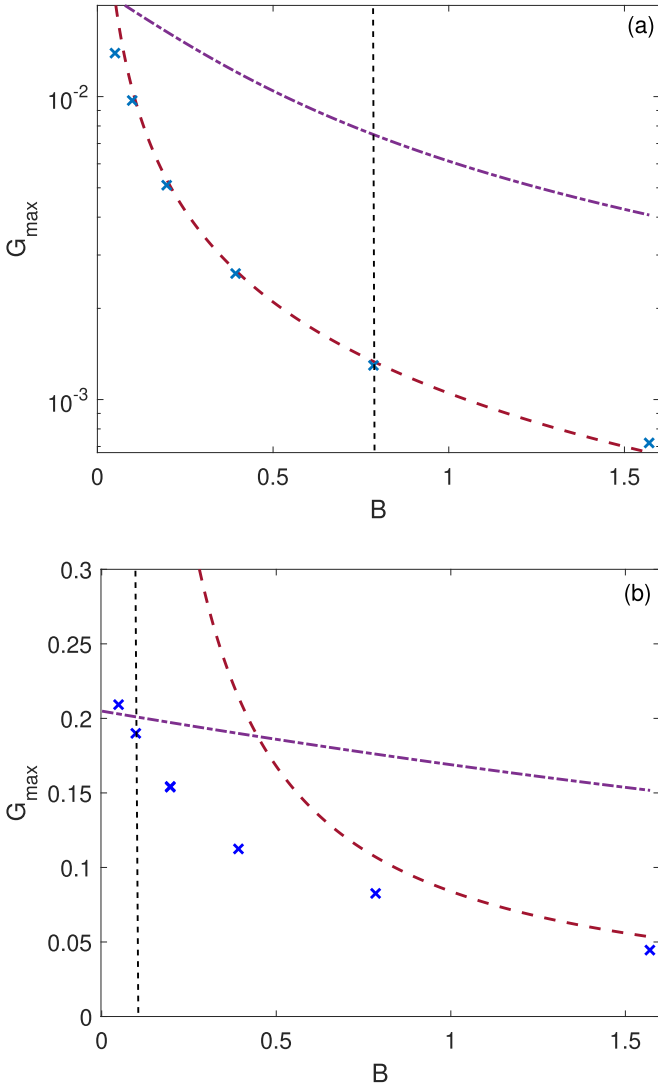
FIG. 5. Maximum gain $G_{max}$ as a function of $B$ at constant $N_0 B$. Same convention as in Fig. 2, dichotomous process excluded. We take a constant $\kappa_0 = 2\pi$ and (a) $N_0 B = 0.0039$, (b) $N_0 B = \pi/10 = 0.314$. Notice the ordinate axis is in logarithmic scale in (a). The dashed vertical lines highlight the values of $B$ used in Figs. 4(a) and 4(b), respectively.

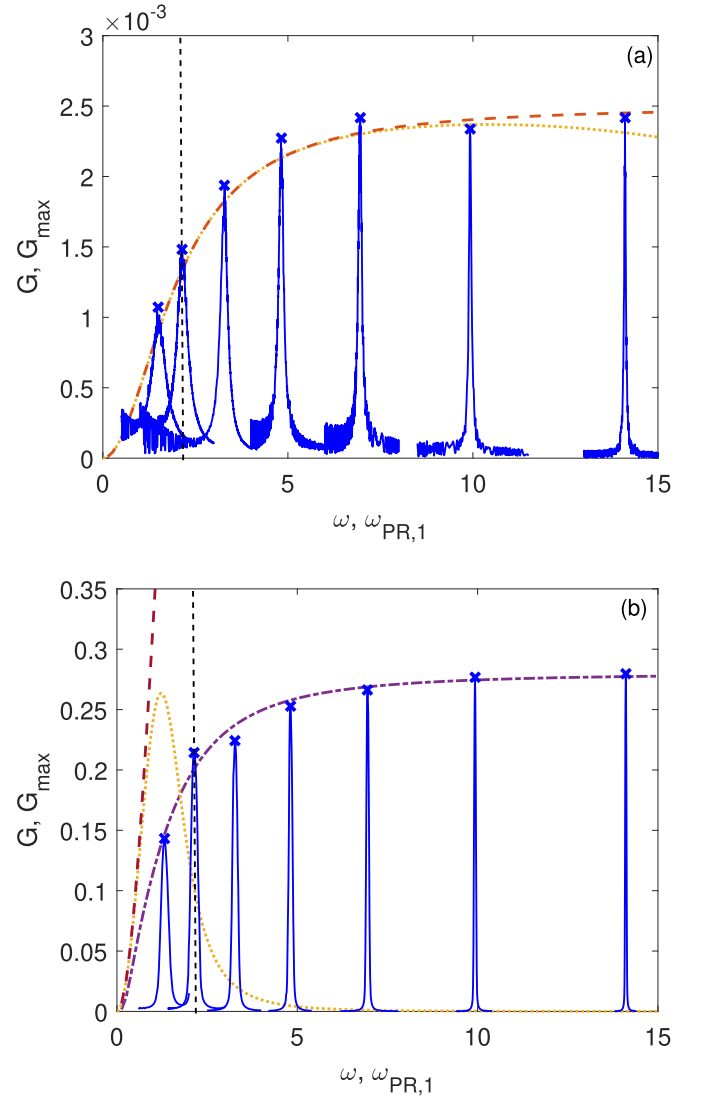

FIG. 6. MI gain curves $G(\omega)$ and their maxima $G_{max}$ obtained for different values of $\kappa_0 \in \{\pi, 2\pi, 4\pi, 8\pi, 16\pi, 32\pi, 64\pi\}$. Comparisons of numerical results (blue crosses and blue solid lines) with the peak of Eq. (26) (red dashed line) and of Eq. (34) [purple dashed-dotted line, not shown in (a), out of scale]. We include also $G_2(\omega)$ for the white-noise limit at the corresponding (yellow dotted line). The dashed vertical lines highlight the value of $\kappa_0$ used in Figs. 4 and 5. (a) $N_0 = 0.005$, $B = \pi/4$; (b) $N_0 = 3.2$, $B = \pi/32$.

significant statistical sample for each value. Only the Gaussian process is considered.

For small $N_0 B = 0.0039$ the MI gain follows very well the cumulant expansion: $G_{max}$ grows for $B \to 0$ (notice the logarithmic scale). The functional approach always overestimates it. For larger $N_0 B = \pi/10$ we still observe a decreasing trend of $G_{max}$. It is apparent that the cumulant expansion is valid only for large $B > \pi/2$ and completely loses its validity below $B = \pi/4$. The functional approach works well in the PR limit, i.e., for $B < \pi/16$. Indeed, $\zeta_c$ depends inversely on $B$ and the approximation is expected to become more faithful. The residual discrepancies may depend on a systematic error of the averaging procedure or on numerical inaccuracies. In brief, we show the transition from the stochastic regime, where the MI gain scales with $N_0$, to the parametric regime where it depends on $\sigma_\xi$, i.e., the fluctuation amplitude.

Finally, we report in Fig. 6 different MI gain curves obtained from numerical simulations of the Gaussian process by varying $\kappa_0 \in \{\pi, 2\pi, 4\pi, 8\pi, 16\pi, 32\pi, 64\pi\}$. The simulation parameters are chosen for each value to ensure that the sample is statically significant.

In Fig. 6(a), we choose $N_0 = 0.005$ and $B = \pi/4$ and show that the MI lobes have a Lorentzian shape dominated by a simple envelope, as predicted by Eq. (25). We explicitly show $G_2^{max}$ obtained from Eq. (26) for the values of $\omega_{PR,1}$ corresponding to a continuous set of $\kappa_0$ (red dashed line) and compare it to the values of $G_{max}$ (blue crosses). They match very well over the full range of $\omega$. The result of the functional approach, Eq. (34), is not shown here because it always overestimates the MI gain. We also include the white-noise gain

for the given $N_0$ (yellow dotted line). For such a small PSD value, it exhibits a monotone growth up to $\omega \approx 9$ [compare to Fig. 1(a)] . The expression in Eq. (26) coincides with it up to this point and tends to $N_0/2$ for $\kappa_0, \omega_{\text{PR},1} \to \infty$. This strengthens the idea that the MI gain of stochastic origin is ruled predominantly by $N_0$, at least for small values.

If, instead, we choose $N_0 = 3.2$ and $B = \pi/32$, we observe [see Fig. 6(b)] that the MI lobes are sharper than a Lorentzian. Their maxima (blue crosses) are well approximated by the functional approximation (purple dashed-dotted line), while the cumulant expansion (red dashed line) always overestimates the MI gain by more than three times. For such a small $B$, Eq. (34) effectively coincides with Eq. (29) (not shown) as expected. As in the previous case, the gain monotonously increases with $\kappa_0$, consistently with the PR nature of the phenomenon [see Eq. (29)]. If we consider the white noise, we see that the MI gain exhibits a narrow lobe, that attains a maximum for $\omega \approx 1.25$ and coincides with (26) only for small detuning, as expected.

As $\kappa_0$ is increased, the modulation period of the process becomes smaller, while $\zeta_c$ is kept constant; thus, the near-resonant approximation performs better for large $\kappa_0$ and the discrepancies observed [Fig. 6(b)] are probably due to a systematic error or residual numerical inaccuracies.

## V. CONCLUSIONS

We discuss the modulational instability in nonlinear optical fibers in which the group-velocity dispersion is randomly modulated. In contrast to the exactly solvable case of white noise or of random kicks, we consider the case of stochastic processes with exponentially decaying autocorrelation function. This is equivalent to a Lorentzian-shaped power spectral density, i.e., the process is *colored*. Two families of colored processes are studied: low pass and band pass. For each family, we consider Gaussian and dichotomous processes.

The distinction between the two stochastic processes turns out to be important in the LP and marginal in the BP case. While for very small perturbation the LP yields very small MI gain, for larger power spectral densities it can yield MI sidelobes larger than the white noise, sitting in the same range of detuning and exhibiting larger gain in the tails. For small bandwidth, the gain disappears, while in the opposite limit it converges to the white-noise limit. The variance demanded for obtaining a measurable MI gain is large, though, and the dichotomous process looks more promising in view of an experimental characterization of the phenomenon because values of bandwidth (correlation length) exist where the gain is quite larger than the white-noise limit.

As far as a BP process is concerned, if the perturbation is large enough, we may observe several MI sidelobes sitting around PR detunings. We focus on the dominant first peak: it converges to the PR sidelobe for small bandwidth and is generally broader and smaller for small correlation lengths.

We compare our numerical results to different analytical approximations, based on the cumulant expansion (as formalized by van Kampen) or the functional (Furutsu-Novikov-Loginov-Shapiro) formulas. While the former is reliable only for small perturbations and small detuning and provides some qualitative estimates elsewhere, the latter provides good results for the dichotomous processes, for which the closure of the system is rigorously obtained.

For both families of correlation functions, the functional method emerges as more reliable and allows us to describe the transition from parametric to stochastic resonances in the BP case. Notwithstanding, the cumulant expansion provides good estimates of the tails of resonant peaks even for relatively small bandwidth values (large correlation length), beyond the expected validity range of the approximation.

Our results pave the way for tailoring MI gain sidebands in optical fibers by means of stochastic GVD fluctuations and suggest the regimes to achieve that. Such fluctuations can be implemented by continuous or discrete variations of fiber specifications.

## APPENDIX: CUMULANT EXPANSION NEAR RESONANCE

In this Appendix we will apply the cumulant expansion to Eq. (30). The cumulant expansion to second order is built by decomposing Eq. (30) as $\kappa_0 \dot{Y} = [A_2 + \Gamma \psi_1 C'_2 + \Gamma \psi_2 C''_2]Y$, with $A_2$, $C_2$, and $C'_2$ as in Eq. (33). As $\psi_{1,2}$ are mutually independent, the expansion is obtained by computing $K_2$ separately for $C'_2$ and $C''_2$, according to Eq. (17), and adding them up.

We obtain

$$\kappa_0 \frac{d\langle Y \rangle}{dz} = \begin{bmatrix} 6d_2\Gamma^2 & 2d_2\beta^2 & 2\Delta^2 - 4\Gamma^2 d_3 \\ 2d_2\beta^2 & 6d_2\beta^2 & -2\Delta^2 + 4\Gamma^2 d_3 \\ 2\Gamma^2 d_3 - \Delta^2 & -2\Gamma^2 d_3 + \Delta^2 & 4\Gamma^2 d_2 \end{bmatrix} \times \langle Y \rangle, \tag{A1}$$

with

$$d_2 \equiv \frac{1}{\kappa_0} \int_0^\infty d\zeta \, R_{\psi_1}(\zeta) \cos \frac{2\Delta^2}{\kappa_0} \zeta = \frac{N_0 B^2}{2\kappa_0} \frac{1}{B^2 + \frac{4\Delta^4}{\kappa_0^2}},$$

$$d_3 \equiv \frac{1}{\kappa_0} \int_0^\infty d\zeta \, R_{\psi_1}(\zeta) \sin \frac{2\Delta^2}{\kappa_0} \zeta = \frac{N_0 B}{2\kappa_0} \frac{\frac{2\Delta^2}{\kappa_0}}{B^2 + \frac{4\Delta^4}{\kappa_0^2}}. \tag{A2}$$

We note that there is here no counterpart to $c_1$ and near PR $\kappa_0 d_2 \approx 2c_2$. The dominant eigenvalue of the matrix in Eq. (A1) is *exactly* $\lambda^* = 8d_2\Gamma^2$, so the instability gain is

$$G_2^{\text{PR}} = \frac{8d_2\Gamma^2}{\kappa_0}, \tag{A3}$$

which attains a maximum $(G_2^{\text{PR}})^{\text{max}} \approx \frac{N_0\omega_{\text{PR},1}^4}{2\kappa_0^2}$, identical to what is found above in Eq. (26).

[1] V. Zakharov and L. Ostrovsky, Modulation instability: The beginning, Phys. D (Amsterdam) **238**, 540 (2009).

[2] V. Bespalov and V. Talanov, Filamentary structure of light beams in nonlinear liquids, Sov. J. Exp. Theor. Phys. Lett. **3**, 307 (1966) [ZhETF Pis ma Redaktsiiu **3**, 471 (1966)].

[3] T. B. Benjamin and J. E. Feir, The disintegration of wave trains on deep water Part 1. Theory, J. Fluid Mech. **27**, 417 (1967).

[4] V. E. Zakharov, Stability of periodic waves of finite amplitude on the surface of a deep fluid, J. Appl. Mech. Tech. Phys. **9**, 190 (1968).

[5] Y. H. Ichikawa, T. Suzuki, and T. Taniuti, Modulation instability of electron plasma wave, J. Phys. Soc. Jpn **34**, 1089 (1973).

[6] K. Tai, A. Hasegawa, and A. Tomita, Observation of Modulational Instability in Optical Fibers, Phys. Rev. Lett. **56**, 135 (1986).

[7] A. L. Berkhoer and V. E. Zakharov, Self excitation of waves with different polarizations in nonlinear media, Sov. J. Exp. Theor. Phys. **31**, 486 (1970) [Zh. Eksp. Teor. Fiz. **58**, 903 (1970)].

[8] R. H. Stolen, J. E. Bjorkholm, and A. Ashkin, Phase-matched three-wave mixing in silica fiber optical waveguides, Appl. Phys. Lett. **24**, 308 (1974).

[9] S. B. Cavalcanti, J. C. Cressoni, H. R. da Cruz, and A. S. Gouveia-Neto, Modulation instability in the region of minimum group-velocity dispersion of single-mode optical fibers via an extended nonlinear Schrödinger equation, Phys. Rev. A **43**, 6162 (1991).

[10] N. J. Smith and N. Doran, Modulational instabilities in fibers with periodic dispersion management, Opt. Lett. **21**, 570 (1996).

[11] M. Droques, A. Kudlinski, G. Bouwmans, G. Martinelli, and A. Mussot, Experimental demonstration of modulation instability in an optical fiber with a periodic dispersion landscape, Opt. Lett. **37**, 4832 (2012).

[12] A. Armaroli and F. Biancalana, Tunable modulational instability sidebands via parametric resonance in periodically tapered optical fibers, Opt. Express **20**, 25096 (2012).

[13] A. Mussot, M. Conforti, S. Trillo, F. Copie, and A. Kudlinski, Modulation instability in dispersion oscillating fibers, Adv. Opt. Photonics **10**, 1 (2018).

[14] F. K. Abdullaev, S. A. Darmanyan, A. Kobyakov, and F. Lederer, Modulational instability in optical fibers with variable dispersion, Phys. Lett. A **220**, 213 (1996).

[15] F. K. Abdullaev, S. A. Darmanyan, S. Bischoff, and M. P. Sørensen, Modulational instability of electromagnetic waves in media with varying nonlinearity, J. Opt. Soc. Am. B **14**, 27 (1997).

[16] F. K. Abdullaev and J. Garnier, Modulational instability of electromagnetic waves in birefringent fibers with periodic and random dispersion, Phys. Rev. E **60**, 1042 (1999).

[17] J. Garnier and F. K. Abdullaev, Modulational instability induced by randomly varying coefficients for the nonlinear Schrödinger equation, Phys. D (Amsterdam) **145**, 65 (2000).

[18] M. Chertkov, I. Gabitov, and J. Moeser, Pulse confinement in optical fibers with random dispersion, Proc. Natl. Acad. Sci. USA **98**, 14208 (2001).

[19] M. Karlsson, Four-wave mixing in fibers with randomly varying zero-dispersion wavelength, J. Opt. Soc. Am. B **15**, 2269 (1998).

[20] M. Farahmand and M. de Sterke, Parametric amplification in presence of dispersion fluctuations, Opt. Express **12**, 136 (2004).

[21] G. Dujardin, A. Armaroli, S. R. Nodari, A. Mussot, A. Kudlinski, S. Trillo, M. Conforti, and S. De Bievre, Modulational instability in optical fibers with randomly kicked normal dispersion, Phys. Rev. A **103**, 053521 (2021).

[22] R. C. Bourret, Propagation of randomly perturbed fields, Can. J. Phys. **40**, 782 (1962).

[23] N. G. Van Kampen, Stochastic differential equations, Phys. Rep. **24**, 171 (1976).

[24] N. G. Van Kampen, A cumulant expansion for stochastic linear differential equations. I, Physica (Amsterdam) **74**, 215 (1974).

[25] N. G. Van Kampen, A cumulant expansion for stochastic linear differential equations. II, Physica (Amsterdam) **74**, 239 (1974).

[26] R. H. Terwiel, Projection operator method applied to stochastic linear differential equations, Physica (Amsterdam) **74**, 248 (1974).

[27] R. F. Fox, Uniform convergence to an effective Fokker-Planck equation for weakly colored noise, Phys. Rev. A **34**, 4525 (1986).

[28] V. N. Kampen, *Stochastic Processes in Physics and Chemistry* (Elsevier, Amsterdam, 2007).

[29] K. Furutsu, On the statistical theory of electromagnetic waves in a fluctuating medium (I), J. Res. Natl. Bur. Stand., Sect. D **67D**, 303 (1963).

[30] E. A. Novikov, Functionals and the random-force method in turbulence theory, Sov. Phys.–JETP **20**, 1290 (1965) [J. Exptl. Theoret. Phys. (U.S.S.R.) **47**, 1919 (1964)].

[31] V. E. Shapiro and V. M. Loginov, "Formulae of differentiation" and their use for solving stochastic equations, Phys. A (Amsterdam) **91**, 563 (1978).

[32] W. Zhang, J. Casademunt, and J. Viñals, Study of the parametric oscillator driven by narrow-band noise to model the response of a fluid surface to time-dependent accelerations, Phys. Fluids A **5**, 3147 (1992).

[33] M. Gitterman, *Noisy Oscillator, The: Random Mass, Frequency, Damping* (World Scientific, Singapore, 2005).

[34] G. P. Agrawal, *Nonlinear Fiber Optics*, 5th ed. (Academic, Oxford, 2012), p. 648.

[35] R. L. Stratonovich, *Topics in the Theory of Random Noise (Vol. 1)*, 1st ed. (Gordon and Breach, New York, 1963).

[36] A. A. Dubkov and O. V. Muzychuk, Analysis of higher approximations of Dyson's equation for the mean value of the Green function, Radiophys. Quantum Electron. **20**, 623 (1977).

[37] M. Gitterman, Classical harmonic oscillator with multiplicative noise, Phys. A (Amsterdam) **352**, 309 (2005).

[38] N. N. Rosanov and V. A. Smirnov, Small-scale self-focusing of laser radiation in amplifier systems, Sov. J. Quantum Electron. **10**, 232 (1980) [Kvantovaya Elektron. (Moscow) **7**, 410 (1980)].

[39] L. D. Landau, *Mechanics: Course of Theoretical Physics* (Volume 1), 3rd ed. (Butterworth-Heinemann, Oxford, 1976), p. 170.

[40] S. Burov and M. Gitterman, Noisy oscillator: Random mass and random damping, Phys. Rev. E **94**, 052144 (2016).